

Full paper

Novel Energy Transfer Mechanism in a Running Quadruped Robot with One Actuator per Leg

Nicholas Cherouvim and Evangelos Papadopoulos*

Department of Mechanical Engineering, National Technical University of Athens,
9 Heroon Polytechniou Street, 15780 Athens, Greece

Received 27 March 2009; accepted 15 June 2009

Abstract

In this work we develop a novel method, or mechanism, of energy transfer in a quadruped running robot. The robot possesses only one actuator per leg, for lower weight and greater power autonomy. The developed mechanism ensures correct dispersion of energy to the actuated and the unactuated degrees of freedom of the robot for stable running. In the mechanism design, we address the added problem of running on inclined ground. In conjunction with a pitch control method, the energy transfer mechanism forms a complete control algorithm. Due to the novel dynamics-based design of the mechanism, it allows the arbitrary setting of the motion forward speed and apex height. Further, it may be applied for different robot physical parameters and ground inclines, without extensive controller tuning. This has not been previously possible using only one actuator per leg. Simulations of a detailed three-dimensional model of the robot demonstrate the mechanism on two different robots. The simulations take into account many real-world characteristics, including realistic leg models, energy loss due to feet collisions, foot-ground friction and energy losses in the joints. Results demonstrate that inclines of up to 20° are properly negotiated.

© Koninklijke Brill NV, Leiden and The Robotics Society of Japan, 2010

Keywords

Legged, energy transfer, running, control

1. Introduction

Biomimetic robots have drawn intense research interest over recent years. A key field of interest is that of quadruped biomimetic legged locomotion. It is well known that animals possess a large number of muscles with which to actuate their limbs and generate stable locomotion. In robotics, on the other hand, the potential for using a large number of actuators is always restricted by considerations of power autonomy and robot weight. Therefore, one of the challenges in legged robots is

* To whom correspondence should be addressed. E-mail: egpapado@central.ntua.gr

how to produce stable, controllable gaits using as few actuators as possible. The quadruped robot designs to date use varying numbers of actuators per leg, from three per leg for the Tekken and BigDog robots, to just one actuator per leg in the case of the Scout II robot [1–3]. The control approaches used for quadruped robots are also varied, and include PD-type control, adaptive and also fuzzy control methods [4–6].

Although using one actuator per robot leg results in a more complex control problem, due to fewer controllable inputs, it also implies that a robot of lower cost, less weight and simpler mechanical design can be achieved. To date, although quadruped robots with just one actuator per leg have run successfully, the associated control algorithms have not been derived from the robot dynamics, and have required trial-and-error estimation of key control parameters. A direct result of this is that the controller requires specific tuning for every different speed of forward motion, as well as for any change in the robot's physical parameters or the ground parameters. Therefore, there is a need for a method of control that is derived from the dynamics of the robot. Such a dynamics-based approach could be applied to robots with varied physical parameters, for various ground inclines, and would allow the arbitrary setting of the forward speed and hopping height of the motion, without retuning of the control parameters. This has not yet been possible with previous control approaches using a single actuator per leg.

In this paper we focus on such a dynamics-based approach through the development of an energy transfer mechanism (ETM) that ensures the proper regulation of energy transfer between the unactuated and actuated degrees of freedom for a quadruped robot with one actuator per leg, shown in Fig. 1a. The ETM is based only on robot dynamics, and requires the feedback of only limb lengths and angles. Further, as more legged systems rely on electric motors for actuation, the ETM is designed to incorporate the effect of motor rotor inertia on the dynamics. Due to the speed reductions used with electric motors this effect is significant and is generally not studied in the control of legged systems. In conjunction with a pitch control algorithm, the ETM can be used to achieve stable running gaits with arbitrary desired forward speeds and apex heights, on level or inclined ground. A case

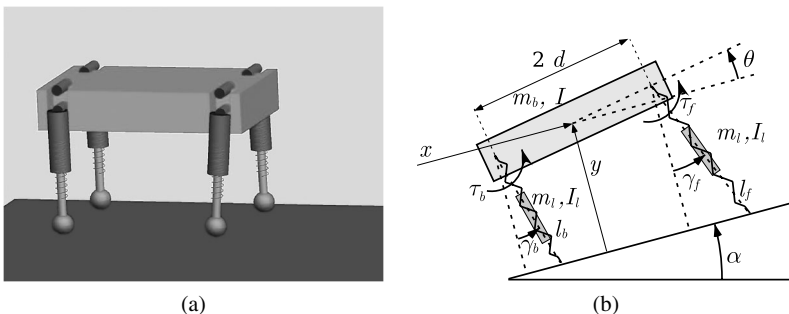


Figure 1. (a) Quadruped robot, with four springy legs and one actuator per leg, located at the hip. (b) Two-dimensional robot model, on an incline.

study, showing that the required torque of steady-state running becomes almost zero on a suitable downhill slope, demonstrates that the ETM utilizes the robot internal dynamics well, since it displays an almost passive gait that is characteristic of semi-passive walkers. The paper begins with a presentation of the robot dynamics, which is followed by the development of the ETM. Results are shown that demonstrate the validity of the ETM on inclined ground, a case study of semipassive motion is presented, and the ability to regulate the robot forward speed and attained apex height to desired values is demonstrated.

2. Robot Model and Dynamics

Consider the quadruped robot depicted in Fig. 1a. The robot has four legs, each of which has a rotary hip joint that is actuated and a prismatic joint that is unactuated, but has a passive spring. As the mechanism of energy transfer involves the vertical and forward modes of motion, we use a two-dimensional (2-D) model of the robot to perform our analysis (Fig. 1b).

The 2-D model captures the relevant dynamic characteristics of the robot in the plane of its forward motion. The model is shown in Fig. 1b on a slope of known incline α , which may be either positive (uphill) or negative (downhill). The body has mass m_b and inertia I with respect to the body center of mass; also see Table 1 for parameters used. Each leg is actuated by a torque at the hip. The body forms an angle θ with respect to the incline.

We focus on the pronking gait as it is symmetric in the third dimension and can be well represented in two dimensions. In the ideal pronking gait the back legs of the robot are in phase, as are the front legs, and the back and front pairs move parallel to one another. The ideal pronking gait has only two discrete phases — the flight phase when the robot is in the air and the stance phase when all the legs are on the ground. In practice, there are usually short phases where only some legs are on the ground.

Table 1.

Variables and indices used in the work

Symbol	Definition	Symbol	Definition
m_b	robot body mass	x	horizontal position of body CoM
k	leg spring stiffness	y	vertical position of body CoM
I	inertia of robot body	θ	pitch angle of body
L	leg rest length	l_i	leg length of leg i
d	half the hip spacing	γ_i	leg angle from vertical, of leg i
b	leg viscous friction coefficient	td	(as index) value at leg touchdown
i_m	inertia of motor rotor	\dot{x}_{des}	desired forward speed
T_{st}	Duration of the stance phase	h_{des}	desired apex height during flight
τ	constant torque applied during stance	γ_{sum}	sum of leg angles

The dynamics for the robot model of Fig. 1b are found using a Lagrangian approach, using the robot body center of mass (CoM) Cartesian coordinates x , y and pitch, θ , as generalized variables. The Cartesian coordinates are taken with reference to the sloped ground. For this reason, in the remainder of the paper we refer to the vertical direction as meaning the direction perpendicular to the sloped ground and the forward direction as the direction parallel to the sloped ground. We write the dynamics for the case where both robot legs are on the ground, as this is the only stance phase in the ideal pronking gait. We do not write the dynamics for the flight phase, as in flight the model is simply a freely falling three-link mechanism, for which the angular momentum is conserved.

The full dynamics for the stance phase are given in the Appendix, taking into account that the effect of the leg inertial properties is negligible during the stance phase, compared to the body inertia effect. As can be seen in the Appendix, the inclusion of the motor rotor inertia i_m introduces extra terms in the mass matrix. By making small angle trigonometric assumptions for the leg angles and body pitch angle, and because the ratio of the magnified rotor inertia $i_m n^2$ over the body mass m_b is small, the mass matrix assumes a diagonal form. Additionally, the rotor inertia introduces several terms on the right hand side of the dynamics, which are neglected as they are small compared to the much stronger spring force terms, viscous friction terms and actuator terms. Therefore, the dynamics in the Appendix become:

$$\begin{aligned} & \left(m_b + i_m n^2 \left(\frac{1}{l_b^2} + \frac{1}{l_f^2} \right) \right) \ddot{x} + k(L - l_b) \sin \gamma_b \\ & \quad + k(L - l_f) \sin \gamma_f - b\dot{l}_b \sin \gamma_b - b\dot{l}_f \sin \gamma_f \\ & = -mg_x - \frac{\tau_b \cos \gamma_b}{l_b} - \frac{\tau_f \cos \gamma_f}{l_f} \end{aligned} \tag{1}$$

$$\begin{aligned} & m_b \ddot{y} - k(L - l_b) \cos \gamma_b - k(L - l_f) \cos \gamma_f + b\dot{l}_b \cos \gamma_b + b\dot{l}_f \cos \gamma_f \\ & = -mg_y - \frac{\tau_b \sin \gamma_b}{l_b} - \frac{\tau_f \sin \gamma_f}{l_f} \end{aligned} \tag{2}$$

$$\begin{aligned} & (I + i_m n^2) \ddot{\theta} + dk(L - l_b) \cos(\gamma_b - \theta) - dk(L - l_f) \cos(\gamma_f - \theta) \\ & \quad - db\dot{l}_b \cos(\gamma_b - \theta) + db\dot{l}_f \cos(\gamma_f - \theta) \\ & = \frac{(d\tau_b \sin(\gamma_b - \theta) - l_b)}{l_b} - \frac{(d\tau_f \sin(\gamma_f - \theta) - l_f)}{l_f}, \end{aligned} \tag{3}$$

where n is the speed reduction of each motor, g_x and g_y are the components of the gravity vector g , parallel and perpendicular to the sloped ground of angle α (Fig. 1b). The incline α changes the effective gravity to g_y in (2) and also introduces g_x in (1), which causes a constant disturbance to the forward dynamics. The incline angle α is positive for uphill ground. The components g_x and g_y are given by:

$$g_x = g \sin \alpha, \quad g_y = g \cos \alpha. \tag{4}$$

The three equations (1)–(3) each represent the dynamics of a particular mode of the robot motion. Equation (1) refers to the robot forward motion mode, while (2) and (3) represent the vertical and pitching motion modes, respectively.

3. ETM

3.1. Problem Statement and Approach

Using only one actuator per leg at each hip allows a simple robot design, but it also introduces the problem of how energy can be transferred from the actuated hip degree of freedom to the unactuated prismatic leg degree of freedom that contains the passive spring. In Ref. [8], the problem has been engaged for the case of a one-leg hopping robot. This transfer of energy is necessary to sustain the vertical oscillation of the body CoM during a running gait, since energy is lost in running due to collisions and friction. This necessity is also apparent from the dynamics in (1)–(3), where it can be seen that there are strong torque inputs available only in the forward and pitching dynamics, as shown in (1) and (3), respectively. The vertical dynamics in (2), on the other hand, show the torque actuator input to be multiplied by the sine of each leg angle (Fig. 1b). Since the legs generally perform small motions around the zero angle, this means that the actuator input to the vertical dynamics will be weak and will often vanish. For this reason, the torque inputs cannot be used to implement the transfer of energy to the vertical dynamics and a different method must be used. In particular, since we are examining the general case where the robot is on a slope, we must also consider the effect of the gravity potential field that adds or removes system energy according to the incline.

To be able to analytically derive the ETM from the robot dynamics, we use some hypotheses, which we clearly lay out below.

- H1 The contribution of the dissipation forces in stance phase forward dynamics, see (1), is negligible.
- H2 To predict the change in forward speed during a stance phase, the behavior of the springy legs in stance is approximated by the simple mass–spring model. The mass is equal to the robot mass and the spring constant is equal to the sum of the robots leg spring constants:

$$m_b \ddot{l}_b = 2k(L - l_b) - m_b g_y. \quad (5)$$

- H3 In the stance dynamics, the leg lengths l_b and l_f are considered equal to the leg rest length L , for terms that involve the input torques τ_b and τ_f .
- H4 In the pronk the back and front legs are almost parallel, so the difference in angles is small.
- H5 For reasonable speeds, the leg angles and body pitch angle are small enough for trigonometric small angle simplifications.

For the derivation of the ETM, we study each robot motion mode separately, i.e., vertical, forward and pitching modes. First, we identify the control inputs to the system. These are the leg touchdown angles, $\gamma_{b,td}$ and $\gamma_{f,td}$, and also the actuator torque applied at the back and front hips, τ_b and τ_f , respectively. In practice, the two leg touchdown angles are not directly controlled in the physical robot, but rather they provide the desired touchdown angles of the individual legs, which are servoed during flight. We determine beforehand that the torque applied by the back and front hip actuators will be constant during stance and equal at the back and front legs:

$$\tau_b = \tau_f = \tau = \text{const.} \quad (\text{in stance}). \quad (6)$$

Therefore, the actuator torques in stance provide only the single input τ . As a result, the three control inputs to the robot are the leg touchdown angle inputs, $\gamma_{b,td}$ and $\gamma_{f,td}$, and the constant torque, τ , applied in stance. Also, for a gait of speed \dot{x} , the leg angle evolution through stance is as predicted by Raibert [9]:

$$\gamma_i = \gamma_{i,td} - \frac{\dot{x}}{L}t, \quad (7)$$

where $i = b, f$, $\gamma_{i,td}$ is the leg touchdown angle and time t starts at leg touchdown.

3.2. Derivation of ETM

First, it should be stated that the ETM involves two of the robot motion modes, i.e., forward and vertical modes, but not the pitching mode and subsequently the pitching motion is not studied here. The pitching mode motion, in gaits like pronking and trotting, is desired to be very limited and does not participate in the mechanism of energy transfer between actuated and unactuated degrees of freedom. However, pitching must be controlled for the gait to be stable and to this end we refer to our previous work [10]. In Ref. [10], we use the difference of the leg touchdown angles, $\gamma_{dif,td}$, to control the robot pitching motion, and although in Ref. [10] the inertia of the motor rotors is not considered and the study is for level ground, it is possible to apply a similar approach for the control of the pitching motion, and this is what we use in the testing of Section 4.

To bring the dynamics into a form suitable for the derivation of the ETM mechanism, we start from the dynamics laid out in (1)–(3). We write the leg lengths as functions of y , θ , γ_b and γ_f (Fig. 1b), and we make use of H1, H3, H4, H5 and (7). Finally, we also take into account that the torque applied during the stance phase is equal at the back and front legs and constant, according to (6). After some algebraic manipulation and making use of simple trigonometric properties, this results in the dynamics of (1)–(3) taking on the form:

$$\left(m_b + \frac{2i_m n^2}{L^2}\right)\ddot{x} + 2k\gamma_b(L - l_b) = -2\frac{\tau}{L} - m_b g_x \quad (8)$$

$$m_b \ddot{y} + 2b\dot{y} + 2ky = -m_b g_y + 2kL \cos\left(\frac{\gamma_{sum,td}}{2} - \frac{\dot{x}t}{L}\right) \cos\left(\frac{\gamma_{dif,td}}{2}\right) \quad (9)$$

$$\begin{aligned}
 & (I + 2i_m n^2)\ddot{\theta} + 2d^2 b\dot{\theta} + 2d^2 k\theta \\
 & = -2\tau + 2kL \sin\left(\frac{\gamma_{\text{sum,td}}}{2} - \frac{\dot{x}t}{L}\right) \sin\left(\frac{\gamma_{\text{dif,td}}}{2}\right), \tag{10}
 \end{aligned}$$

where $\gamma_{\text{sum,td}}$ is the sum of the leg touchdown angles and $\gamma_{\text{dif,td}}$ is the difference of the leg touchdown angles. Also, for more compact mathematics, we define the quantities m_{bx} , $m_{b\theta}$ as:

$$m_{bx} = m_b + \frac{2i_m n^2}{L^2}, \quad m_{b\theta} = I + 2i_m n^2. \tag{11}$$

Observing the simpler form of the dynamics in (8)–(10), it is interesting to recap on the energy transfer problem. As mentioned above, the actuator input to the dynamics is strong in the forward and pitching motions, and absent in the vertical motion mode. On the other hand, the vertical dynamics includes strong viscous friction terms, which will erode the robot oscillation. Therefore, the ETM is needed to pump energy into the vertical dynamics, whilst also ensuring that the robot achieves a desired forward speed and a desired apex height during flight.

According to H4, the effect of $\gamma_{\text{dif,td}}$, on the vertical dynamics in (9) will be very limited, due to the cosine. As a result, focusing only on the forward and vertical dynamics, we have:

$$m_{bx}\ddot{x} + 2k\gamma_b(L - l_b) = -2\frac{\tau}{L} - mg_x \tag{12}$$

$$m_b\ddot{y} + 2b\dot{y} + 2ky = -m_b g_y + 2kL \cos\left(\frac{\gamma_{\text{sum,td}}}{2} - \frac{\dot{x}t}{L}\right). \tag{13}$$

Energy can easily be added to the forward dynamics by using the actuator torque. An important difference between this model and others, such as Raibert’s earlier approach, is that the robot carries only one actuator per leg and therefore the vertical mode of motion is completely unactuated. The challenge is to transfer energy provided by the hip actuator torque to the vertical mode described by (13). To do this, we first look at the vertical mode of motion and then we turn to the forward mode.

To ensure that the energy associated with the vertical motion of the robot is correct, it is necessary to determine a criterion according to which the energy will be considered sufficient. We use the apex height that the robot reaches during the flight phase to determine whether sufficient energy is present in the vertical dynamics. To do this we consider a desired apex height, h_{des} , that is built into the ETM and can be set by the robot user. Note that the apex height is not explicitly needed as feedback.

We can see that the vertical dynamics in (13) is represented by a driven oscillator. The driving term does not contain the actuator torque τ , but rather the sum of the leg touchdown angles $\gamma_{\text{sum,td}}$. Therefore, we use $\gamma_{\text{sum,td}}$ as a control input to the vertical dynamics. With some extensive algebra, it is possible, given the state of the robot at a touchdown event, to solve the dynamics in (13) and compute the required sum of the leg touchdown angles, such that the vertical velocity of the robot body at

liftoff has a desired value \dot{y}_{10} . Being able to determine the vertical velocity at liftoff is equivalent to being able to determine the apex height the robot will reach during flight, as in flight the robot CoM executes a ballistic motion. After some algebra, the sum of the leg touchdown angles may be computed as a function of the robot state at the previous liftoff and this provides the first ETM equation:

$$\gamma_{\text{sum,td}} = f(\dot{x}_{\text{des}}, h_{\text{des}}, \text{robot parameters, state of the robot at liftoff}). \quad (14)$$

The state of the robot at liftoff is computed by using feedback from leg lengths and angles, and their corresponding velocities, as well as the pitch and pitch velocity. Of these, the leg lengths and angles are straightforward to measure, while a high-bandwidth method for measuring pitch is presented in Ref. [11].

Equation (14) uses the sum of the leg touchdown angles to regulate the energy inserted into the vertical dynamics. If more energy is required in the vertical degree of freedom, then $\gamma_{\text{sum,td}}$ will be increased. Essentially this forces a more aggressive angle of attack for the leg upon touchdown, which causes greater compression of the spring due to the forward motion of the robot. Therefore, energy is taken from the forward motion, stored in the spring and then released upon liftoff, where it translates into the attained apex height.

Since the ETM makes use of the robot's forward energy to pump energy into the vertical degree of freedom, it is now necessary to regulate the energy associated with the forward motion of the robot. Otherwise the robot would progressively accelerate or decelerate in an uncontrolled fashion, resulting in failure of the gait. Equation (12) shows that the forward dynamics involve the constant torque applied during stance, τ . We use this torque input to bring the forward speed of the robot at touchdown to the desired forward velocity, by the liftoff event. To do this, we first express the forward velocity of the robot at liftoff as a function of the touchdown forward velocity. This can be accomplished by using H4, according to which the sum of the touchdown angles $\gamma_{\text{sum,td}}$ in the pronking gait is equal to twice one of $\gamma_{\text{b,td}}$, $\gamma_{\text{f,td}}$. Also, utilizing (7), and integrating (12) once, the forward speed \dot{x}_{i+1} after stance can be computed, given the speed before stance, \dot{x}_i , as a function of the control inputs $\gamma_{\text{sum,td}}$, τ :

$$\dot{x}_{i+1} = -k \int_0^{T_{\text{st}}} \frac{1}{m_{\text{bx}}} \left(\gamma_{\text{sum,td}} - 2 \frac{\dot{x}_{\text{dest}}}{L} \right) (L - l_{\text{b}}) dt - \frac{2}{m_{\text{bx}} L} \tau T_{\text{st}} + \dot{x}_i. \quad (15)$$

As can be seen, the forward speed of the robot at liftoff can be controlled by selecting the constant torque τ applied during the stance phase. From (15), using H2 and having computed $\gamma_{\text{sum,td}}$ from (14), we can find the second equation of the ETM that provides the torque τ to be applied during stance:

$$\tau = f(\dot{x}_{\text{des}}, h_{\text{des}}, \gamma_{\text{sum,td}}, \text{robot parameters, state of robot at liftoff}). \quad (16)$$

Overall, the ETM provides the inputs $\gamma_{\text{sum,td}}$ and τ , from (14) and (16), while the pitching control from Ref. [10] provides the input $\gamma_{\text{dif,td}}$. As a result, we know both individual leg touchdown angles, $\gamma_{\text{b,td}}$ and $\gamma_{\text{f,td}}$, and the constant torque, τ , that must be applied by the hip actuators during stance.

4. Results

In this section we evaluate the performance of the ETM for pronking on sloped ground of various inclines. As explained in the previous section, the ETM is used in conjunction with the pitch control method from Ref. [10]. In this way the robot can be controlled to a desired forward speed with a desired apex height. To begin each motion the robot always starts from an initial height with zero forward speed. The exact height the robot starts from is not critical and as can be seen from the simulation results the robot can overcome considerable deviations of the initial conditions from the desired steady state gait.

For the purpose of testing the ETM in realistic conditions, the ETM is applied to a full robot model, which is much more complex than the model of Section 2 and includes many real-world characteristics. It is clear that the model simulated takes into account many factors that are not included in the model used for the design of the ETM. A typical example is the fact that the simulated model uses discrete masses for all main parts of the robot, whereas the model used for the ETM design has only the body mass. Essentially, applying the ETM to the simulated model also tests its performance in the case of modeling error and parametric uncertainty, as would be the case when applying the control to a real robot. The full model includes a detailed leg model, with each leg being comprised of three discrete parts, that all have realistic mass. Also, a Coulomb friction model is included that simulates slipping of the robot foot on the ground, if slipping conditions are met. The impacts of the feet are modeled as plastic collisions. The actuators are considered to be electric DC motors, coupled with planetary gearheads, and a proper motor model is included based on the specific motor torque-speed characteristic and maximum allowable currents, taking data from Ref. [12]. A similar type of approach has been shown to successfully predict the behavior of the Scout II robot [13]. We make use of two variations of the full robot model with different values for key parameters, i.e. robots A and B (Table 2).

The DC motors used are from Maxon motors — motor RE30 for robot A and the stronger motor RE35 for the heavier robot B. In the results, note that negative actuator torques represent torques that accelerate the robot forwards, when in stance. Simulations are performed using the ADAMS software.

4.1. Evaluation of ETM on Sloped Ground

The ETM is first applied to robot A (Table 2), for pronking up a 10° hill. The response is shown in Fig. 2.

In Fig. 2a, the forward speed of the robot is shown to follow the desired speed trajectory very well. It is important to note that the target value for the forward speed is the forward speed during the flight phase of the robot. During the stance phases there is a natural deceleration due to the leg spring compression. Therefore, the robot forward speed should coincide with the desired speed trajectory only during each flight phase, i.e. at the largest forward velocity value during each cycle of motion. This is indeed seen to be the case in Fig. 2a. In Fig. 2b, the apex height

Table 2.

Parameters of the two robots used for testing

Parameter	Units	Robot A	Robot B
Robot body mass, m_b	kg	8	12
Leg mass, for each leg	kg	0.4	0.4
Leg spring stiffness, k	N/m	3500	5000
Leg rest length, L	m	0.3	0.3
Hip spacing, $2d$	m	0.5	0.4
Leg viscous friction coefficient, b	Ns/m	2.5	5.0
Inertia of DC motor rotor, i_m	g cm ²	33.3	72.0
Torque constant of DC motor	Nm/A	0.0292	0.0525
Gear reduction, n	—	51	51
Coulomb static friction coefficient	—	2.0	2.0
Coulomb kinetic friction coefficient	—	0.8	0.8

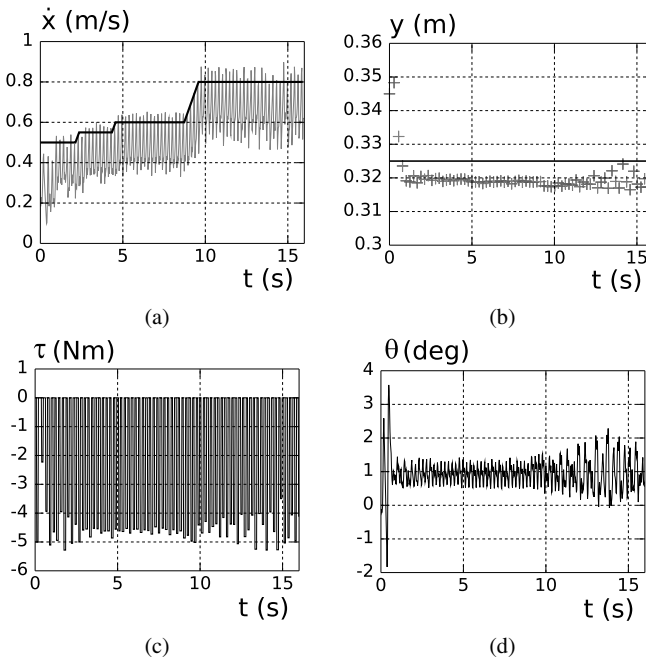


Figure 2. Robot A running on a 10° uphill incline: (a) robot forward speed and desired speed trajectory, (b) body height attained at each apex and desired value (continuous line), (c) torque applied at the back left motor, and (d) pitching of the robot body.

attained by the robot is shown. The small deviation from the desired value is due to the additional complexity of the simulated model compared to the model used for the ETM design. The torque applied by the back left motor during stance is shown in Fig. 2c, and it can be seen that the values are within reasonable limits. Finally,

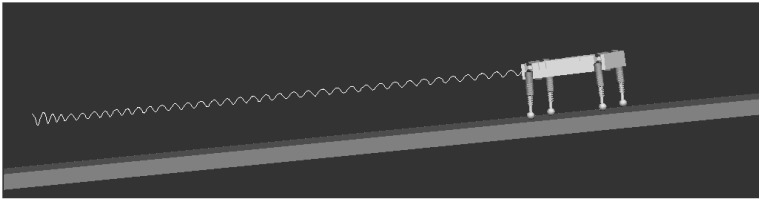


Figure 3. Robot A running on an uphill slope of 5° in ADAMS simulation software. The trajectory of the body CoM is shown.

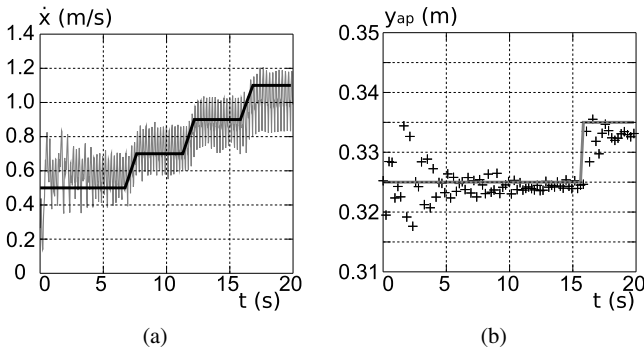


Figure 4. Robot A on -10° incline: (a) forward speed and desired speed trajectory (continuous line), and (b) body height at the apex of each flight phase and the desired height trajectory (continuous line).

the pitch angle of the robot body is shown in Fig. 2d, which is controlled to small values. Additionally, in Fig. 3, the simulation in ADAMS is shown for robot A running up a 5° hill.

A downhill case is also presented using robot A, for a slope of -10° . The response is shown in Fig. 4, although the pitch and torque graphs are omitted for space economy. As in the uphill case, the forward speed trajectory is followed well (Fig. 4a). In Fig. 4b, the apex height of the robot is shown to follow a desired trajectory.

Finally, the second robot, robot B is made to run up a 5° hill and the response is shown in Fig. 5. In this case also, both the forward speed and the apex height attained during flight are successfully made to follow desired trajectories (Fig. 5a and 5b). As mentioned above in the first example, the forward speed of the robot being mainly below the desired trajectory is expected and not a control performance error. The key parameters of robots A and B are very different, and yet the ETM is directly applied to both and performs equally well.

4.2. Effect of Slopes on ETM Inputs

The ETM is completely implemented using the inputs of the sum of the leg touchdown angles, $\gamma_{\text{sum,td}}$, and the constant torque applied during stance, τ . It is interesting to study how different inclines affect the ETM inputs and how this imposes limits on the motion of a given robot. First, we examine the behavior of the con-

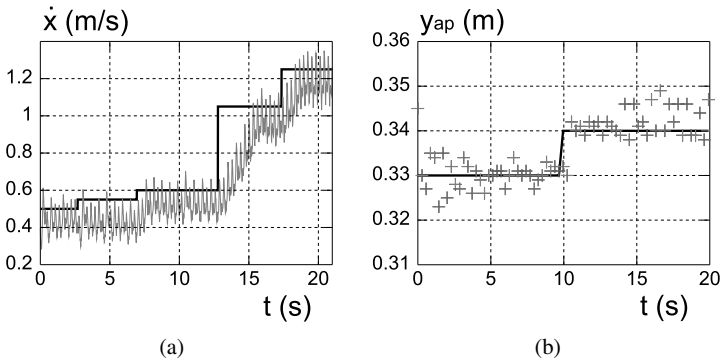


Figure 5. Robot B running up a 5° hill: (a) robot forward speed and desired speed trajectory, and (b) body height attained at each apex and desired trajectory.

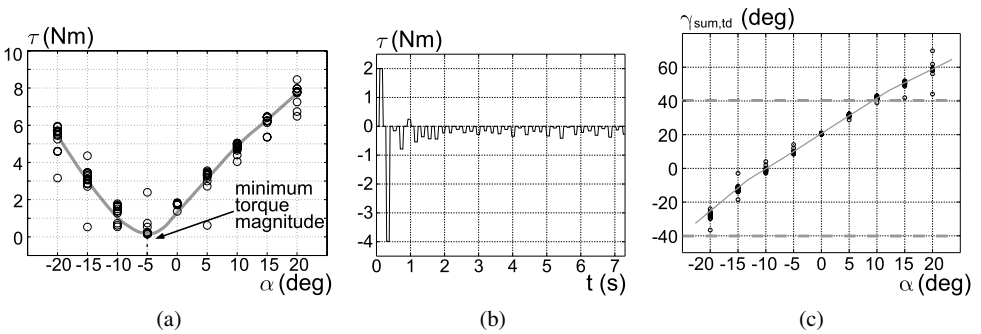


Figure 6. (a) Magnitude of torque applied during the stance phase, for robot A, for various ground inclines α . The data is shown using circles. The arrow shows the required torque with the minimum magnitude for an incline of -6° . (b) Torque applied during stance on a slope of -6° . (c) Sum of the leg angles at touchdown for various inclines α . The data is shown using circles. The dashed lines show limits of 40° .

stant torque τ for different slope inclines. We consider robot A (Table 2). We run the robot with a constant desired forward speed equal to 0.55 m/s, and a constant apex height of 0.32 m. The robot is always left to run for 25 cycles, so that it may enter the steady state. In Fig. 6a, the magnitude of the actuator torque applied during stance is shown, where some distribution of the stance torque is apparent over a range of torque values, for each specific incline angle α . This distribution represents the robot’s transient response before it reaches steady state. The concentrated values of torque represent the steady-state torques applied during stance. Figure 6a shows the torque magnitude, where the torques will be braking for the extreme downhill inclines and propulsive for the steep uphill slopes. It is evident from Fig. 6a that running downhill can be equally demanding in torque as uphill running. Given the maximum actuator torque, it is possible to find the steepest slopes, for both uphill and downhill, that the robot could negotiate.

In Fig. 6a there exists a torque minimum at about 6° of downhill slope and it is interesting that this minimum is close to the zero value. This means that in this case the control consumes much less energy during stance, during the steady-state motion. During flight, of course, regular PD control torques position the legs to their touchdown angles. The fact, however, that the minimum torque point is close to zero is an indication that the ETM utilizes the passive dynamics of the robot well. Essentially, the ETM transfers the energy gained from the robot mass moving through the gravitational potential to the dissipative elements of the system, which are the prismatic joints with viscous leg friction and the collisions of the feet with the ground. This has been observed extensively in passive or semipassive systems, such as passive walkers that may walk down a slope with no actuation at all or a one-legged model that hops with very small effort [14–16]. To date, we are not aware of a previous method for achieving a semipassive run on a quadruped robot, especially with as many sources of losses and using only one actuator per leg. This result is verified by running the particular robot on a downhill slope of 6° and observing the actuator torque that is shown in Fig. 6b.

Now, we examine how the second control input, the sum of the touchdown angles $\gamma_{\text{sum,td}}$, varies with the ground incline. For the same setup as used for Fig. 6a, the control input $\gamma_{\text{sum,td}}$ is plotted *versus* the incline in Fig. 6c. The required sum of the touchdown angles increases as the angle of the ground increases. This result imposes a limit on the steepest slope that the robot can negotiate both in the uphill and the downhill case, due to the possibility of slipping. Larger leg touchdown angles, either positive or negative, are more prone to lead to slipping of the feet. Although the condition for slipping is a function of the applied torque and the leg angles, it is often more practical to simply limit the robot leg touchdown angles. If such a limit for $\gamma_{\text{sum,td}}$ was found to be 40° off vertical, then according to Fig. 6c the robot could run on inclines between -25 and $+10^\circ$.

5. Conclusions

An ETM was presented that is capable of regulating the energy through the robot degrees of freedom, such that both the forward speed and the apex height of a quadruped robot pronking on sloped ground can be controlled, using only one actuator per robot leg. It was seen that slopes of up to 20° could be negotiated, both uphill and downhill. The mechanism was demonstrated to perform well in detailed simulations that included many real-world characteristics, such as leg mass, foot slipping, DC motor models, etc. The problem of pronking on inclined ground was also studied parametrically. From the parametric study of how the incline influenced the required control inputs, the ETM was shown to be making good use of the robot passive dynamics. Finally, the study also uncovered limiting factors, with regard to the applied torque and the leg touchdown angles, that should be considered when running on inclined terrain.

Acknowledgements

This work was cofunded by public funds (European Social Fund 80% and General Secretariat for Research and Technology 20%) and private funds (Zenon SA), within measure 8.3 of Op.Pr.Comp., 3rd CSP-PENED 2003.

References

1. Z. Zhang, Y. Fukuoka and H. Kimura, Adaptive running of a quadruped robot using delayed feedback control, in: *Proc. IEEE Int. Conf. on Robotics and Automation*, Barcelona, pp. 3750–3755 (2005).
2. M. Buehler, R. Playter and M. Raibert, Robots step outside, in: *Proc. Int. Symp. Adaptive Motion of Animals and Machines*, Ilmenau (2005).
3. D. Papadopoulos and M. Buehler, Stable running in a quadruped robot with compliant legs, in: *Proc. IEEE Int. Conf. Robotics and Automation*, San Francisco, CA, pp. 444–449 (2000).
4. S. Talebi, I. Poulakakis, E. Papadopoulos and M. Buehler, Quadruped robot running with a bounding gait, in: *Proc. 7th Int. Symp. on Experimental Robotics*, Honolulu, HI, pp. 281–289 (2000).
5. Y. Fukuoka, H. Kimura and A. H. Cohen, Adaptive dynamic walking of a quadruped robot on irregular terrain based on biological concepts, *Int. J. Robotics Res.* **22**, 187–202 (2003).
6. W. Marhefka, D. E. Orin, J. P. Schmiedeler and K. J. Waldron, Intelligent control of quadruped gallops, *IEEE/ASME Trans. Mechatron.* **8**, 446–456 (2003).
7. K. N. Murphy and M. H. Raibert, Trotting and bounding in a planar two-legged model, in: *Proc. 5th Symp. on Theory and Practice of Robots and Manipulators*, A. Morecki, G. Bianchi, K. Kedzior (Eds), pp. 411–420. MIT Press, Cambridge, MA (1984).
8. N. Cherouvim and E. Papadopoulos, Single actuator control analysis of a planar hopping robot, in: *Proc. Robotics: Science and Systems*, Cambridge (2005).
9. M. H. Raibert, *Legged Robots that Balance*. MIT Press, Cambridge, MA (1986).
10. N. Cherouvim and E. Papadopoulos, Speed and height control for a special class of running quadruped robots, in: *Proc. IEEE Int. Conf. on Robotics and Automation*, Pasadena, CA, pp. 805–810 (2008).
11. J. Leavitt, A. Sideris and J. E. Bubrow, High bandwidth tilt measurement using low-cost sensors, *IEEE/ASME Trans. Mechatron.* **11**, 320–327 (2006).
12. Maxon Motor AG. Available online at www.maxonmotor.com
13. I. Poulakakis, J. A. Smith and M. Buehler, Modeling and experiments of untethered quadrupedal running with a bounding gait: the Scout II robot, *Int. J. Robotics Res.* **24**, 239–256 (2005).
14. T. McGeer, Passive dynamic walking, *Int. J. Robotics Res.* **9**, 62–82 (1990).
15. M. Ahmadi and M. Buehler, Stable control of a simulated one-legged running robot with hip and leg compliance, *IEEE Trans. Robotics Automat.* **13**, 96–104 (1997).
16. R. Tedrake, T. W. Zhang, M. Fong and H. S. Seung, Actuating a simple 3D passive dynamic walker, in: *Proc. IEEE Int. Conf. on Robotics and Automation*, New Orleans, LA, pp. 4656–4661 (2004).

Appendix

The dynamics of the planar model shown in Fig. 1b, including the effect of the rotor inertia of the motors and for the stance phase when both the robot legs are on the ground, have the form:

$$\mathbf{M}[\ddot{x} \quad \ddot{y} \quad \ddot{\theta}]^T = \mathbf{f}, \tag{A.1}$$

where the mass matrix \mathbf{M} is a 3×3 symmetric matrix, with elements:

$$m_{11} = m_b + i_m n^2 \left(\frac{\cos^2 \gamma_b}{l_b^2} + \frac{\cos^2 \gamma_f}{l_f^2} \right)$$

$$m_{12} = i_m n^2 \left(\frac{\cos \gamma_b \sin \gamma_b}{l_b^2} + \frac{\cos \gamma_f \sin \gamma_f}{l_f^2} \right)$$

$$m_{13} = i_m n^2 \left(\frac{\cos \gamma_b (l_b - d \sin(\gamma_b - \theta))}{l_b^2} + \frac{\cos \gamma_f (l_f - d \sin(\gamma_f - \theta))}{l_f^2} \right)$$

$$m_{22} = m_b + i_m n^2 \left(\frac{\sin^2 \gamma_b}{l_b^2} + \frac{\sin^2 \gamma_f}{l_f^2} \right)$$

$$m_{23} = i_m n^2 \left(\frac{\sin \gamma_b (l_b - d \sin(\gamma_b - \theta))}{l_b^2} + \frac{\sin \gamma_f (l_f - d \sin(\gamma_f - \theta))}{l_f^2} \right)$$

$$m_{33} = I + i_m n^2 \left(\frac{(l_b - d \sin(\gamma_b - \theta))^2}{l_b^2} + \frac{(l_f - d \sin(\gamma_f - \theta))^2}{l_f^2} \right)$$

and

$$m_{21} = m_{12}, \quad m_{31} = m_{13}, \quad m_{32} = m_{23}.$$

The right-hand side of the dynamics is $\mathbf{f} = [f_1 \quad f_2 \quad f_3]^T$, where:

$$f_1 = -k(L - l_b) \sin \gamma_b - k(L - l_f) \sin \gamma_f + b \dot{l}_b \sin \gamma_b$$

$$+ b \dot{l}_f \sin \gamma_f - m g_x - \frac{\tau_b \cos \gamma_b}{l_b} - \frac{\tau_f \cos \gamma_f}{l_f}$$

$$+ \frac{i_m n^2 \cos \gamma_b (d \cos(\gamma_b - \theta) \dot{\theta}^2 + 2 \dot{l}_b \dot{\gamma}_b)}{l_b^2}$$

$$+ \frac{i_m n^2 \cos \gamma_f (2 \dot{l}_f \dot{\gamma}_f - d \cos(\gamma_f - \theta) \dot{\theta}^2)}{l_f^2}$$

$$f_2 = k(L - l_b) \cos \gamma_b + k(L - l_f) \cos \gamma_f - b \dot{l}_b \cos \gamma_b$$

$$- b \dot{l}_f \cos \gamma_f - m g_y - \frac{\tau_b \sin \gamma_b}{l_b} - \frac{\tau_f \sin \gamma_f}{l_f}$$

$$+ \frac{i_m n^2 \sin \gamma_b (d \cos(\gamma_b - \theta) \dot{\theta}^2 + 2 \dot{l}_b \dot{\gamma}_b)}{l_b^2}$$

$$\begin{aligned}
& + \frac{i_m n^2 \sin \gamma_f (2\dot{l}_f \dot{\gamma}_f - d \cos(\gamma_f - \theta) \dot{\theta}^2)}{l_f^2} \\
f_3 = & -dk(L - l_b) \cos(\gamma_b - \theta) + dk(L - l_f) \cos(\gamma_f - \theta) \\
& + db\dot{l}_b \cos(\gamma_b - \theta) - db\dot{l}_f \cos(\gamma_f - \theta) \\
& + \frac{(d\tau_b \sin(\gamma_b - \theta) - l_b)}{l_b} \\
& + \frac{i_m n^2 (l_b - d \sin(\gamma_b - \theta))(d \cos(\gamma_b - \theta) \dot{\theta}^2 + 2\dot{l}_b \dot{\gamma}_b)}{l_b^2} \\
& - \frac{(d\tau_f \sin(\gamma_f - \theta) - l_f)}{l_f} \\
& - \frac{i_m n^2 (l_f + d \sin(\gamma_f - \theta))(d \cos(\gamma_f - \theta) \dot{\theta}^2 - 2\dot{l}_f \dot{\gamma}_f)}{l_f^2}.
\end{aligned}$$

About the Authors



Nicholas Cherouvim received his Diploma and PhD from the National Technical University of Athens (NTUA), in 2003 and 2009, respectively, both in Mechanical Engineering. During his undergraduate course he followed the program of study emphasizing mechanical design and control systems. After completing an undergraduate thesis on the energy consumption of legged robots in November 2003, he received the degree of Mechanical Engineer and graduated fifth among 191 graduates that year. He continued as a Researcher in the Control Systems Laboratory, under Professor Evangelos Papadopoulos. His research was on the dynamics and control of legged robots, during which he developed two legged robot platforms. One of these was the SAHR (Single Actuated Hopping Robot), which to the best of his knowledge is the first one-legged robot using only one actuator that was able to negotiate unknown rough terrain. He successfully defended his PhD thesis in May 2009. Research areas that interest him are robotics, mechatronics, control and dynamic systems. He is currently working in industrial research and development. He is a Member of the IEEE and the Technical Chambers of Greece (TEE).



Evangelos Papadopoulos received his Diploma from the National Technical University of Athens (NTUA), in 1981, and his MS and PhD degrees from MIT, in 1983 and 1991, respectively, all in Mechanical Engineering. He was an analyst with the Hellenic Navy, Athens, Greece, from 1985 to 1987. In 1991, he joined McGill University and the Center for Intelligent Machines (CIM) as an Assistant Professor and was tenured in 1997. Currently, he is Professor with the Mechanical Engineering Department at the NTUA. He teaches courses in the areas of systems, control, mechatronics and robotics. His research interests are in the area of robotics, modeling and control of dynamic systems, mechatronics, and design. He serves as an Associate Editor for *Machine and Mechanism Theory*, while previously he served as an Associate Editor for *IEEE Transactions on Robotics* and as a Guest Editor to *IEEE/ASME Transactions on Mechatronics*. He has published more than 150 technical articles in journals and refereed conference proceedings. He is a Senior Member of the IEEE and AIAA, and a member of the ASME, IFToMM, Technical Chamber of Greece (TEE) and Sigma Xi.